S1   Numerical weather prediction model performances
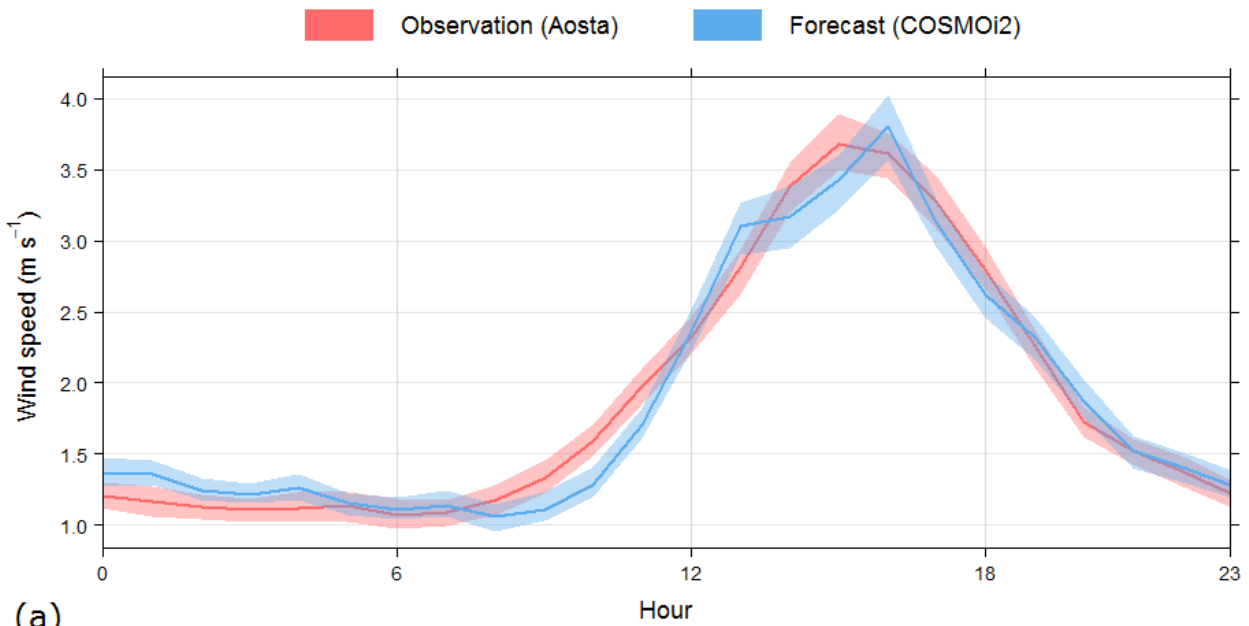
(a)
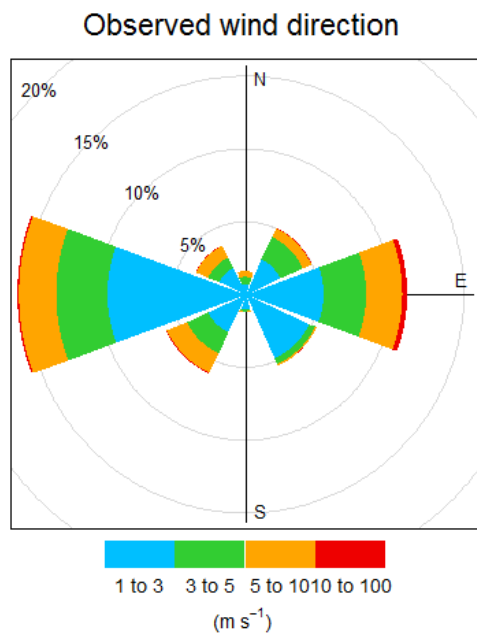
(b)
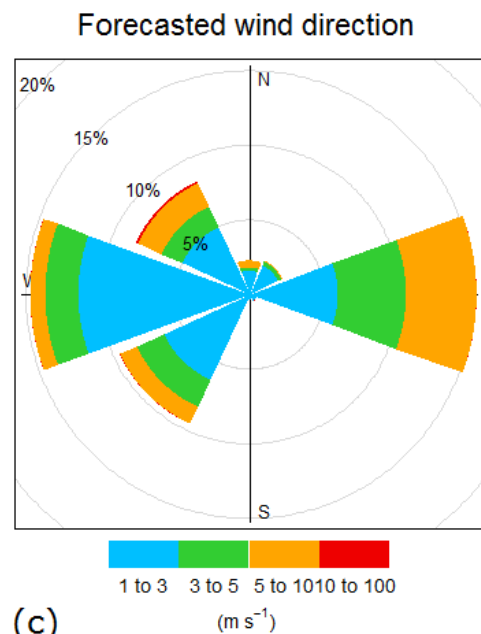
(c)

Figure S1: Comparison between average (2015–2016) wind observations at the Aosta–Downtown weather station and forecasts by COSMO-I2 for the corresponding grid cell. (a) Daily cycle of wind speed. The effect of regular winds blowing in the afternoon, especially the plain-mountain winds, is detectable as a peak between 12 and 18 LT. (b,c) Observed and forecasted wind direction. The distance from the centre of the wind rose identifies the frequency of each class of wind speed (colours) and provenance direction (polar angle).

S2 Details on the regional emission inventory

The Aosta Valley emission inventory is managed by ARPA and is currently updated to 2015. Emissions of pollutants are estimated from the best available understanding of the local sources weighted by appropriate emission factors. The latter are generally taken from the Atmospheric Emission Inventory Guidebook (EEA, 2016), unless more specific or up-to-date information is applicable based on the expertise of the operator and knowledge of the processes acting on a regional scale. The Aosta Valley inventory and the emission calculation methodologies were successfully compared to their national equivalents during an Italian comparison exercise (Pignatelli et al., 2007) in the framework of the Regional Air Pollution Information and Simulation (RAINS) European Program, aimed at harmonizing the European emissions inventories and the calculation methodologies.

In the last inventory (2015), the PM_{10} emissions in the Aosta Valley were evaluated in 690 tonnes/year, mainly attributed to domestic heating emissions (74%). Other contributors are road and off-road transports (15%) and agriculture or farming activities (11%).

S3 Details on the boundary conditions

The boundary conditions employed for this study at an intermediate (Italian and European) scale are provided by the system QualeAria (`http://www.aria-net.it/qualearia/en/`; Menut and Bessagnet (2010); Kukkonen et al. (2012)). The Global Forecast System (GFS) synoptic-scale weather forecasts from the National Center for Environmental Prediction (NCEP) are given as meteorological inputs to QualeAria. The outer air quality boundary conditions are taken from the global scale forecasts provided daily by the ECMWF MACC-C-IFS-TM5 model as part of the Copernicus Atmosphere Monitoring Service (CAMS; `http://macc.copernicus-atmosphere.eu/oper_info/nrt_info_for_users/`). The national and European emissions inventories are distributed by the Italian Institute for Environmental Protection and Research (ISPRA; Taurino et al. (2016)) for Italy and by the TNO/MEGAPOLI project for Europe (`http://megapoli.dmi.dk`, Baklanov et al. (2010)).

The described configuration was successfully tested in previous studies on air quality forecasts in the Aosta Valley (e.g., Silibello et al., 2007; Pession et al., 2008, 2016).

S4 Supporting material to case study 1
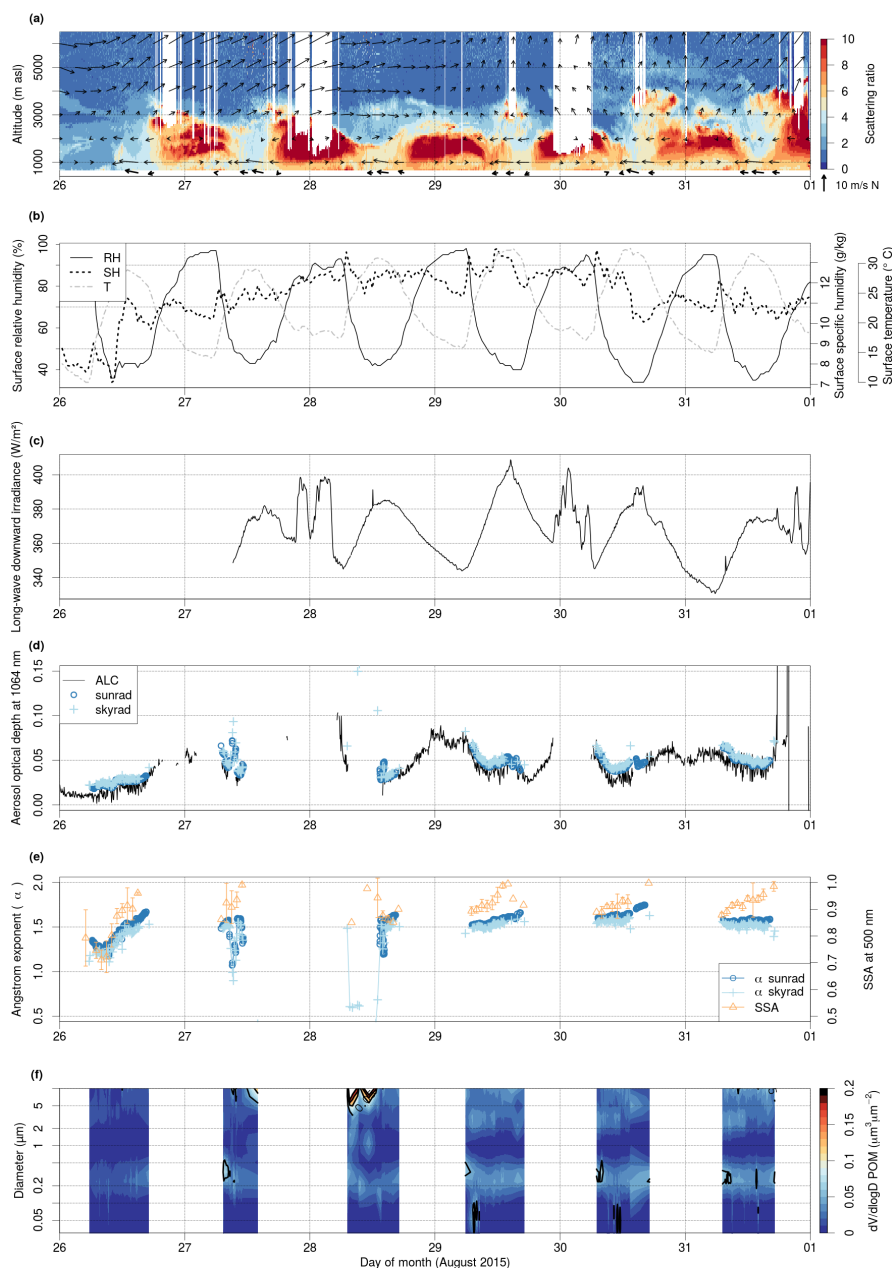
Figure S2: Case study of 26–31 August 2015. (a) Same as in Fig. 4 in the main paper; (b) Surface relative humidity (RH), specific humidity (SH) and temperature (T) measured at the Aosta–Saint Christophe weather station; (c) Downward infrared irradiance measured at Aosta–Saint Christophe. Some of the infrared irradiance spikes occur at the same time as clouds in panel (a) and reveal the quick transition from the aerosol to the cloud phase; (d) AOD at 1064 nm from ALC (derived from the functional relationships and filtered for clouds) and photometer (both sunrad and skyrad algorithms); (e) Ångström exponent from both sunrad and skyrad algorithms (left axis), and SSA (right axis) from the photometer; (f) Volume size distribution from the photometer (cut at 10 μm diameter for ease of visualisation of the smallest sizes).

26 August 2015
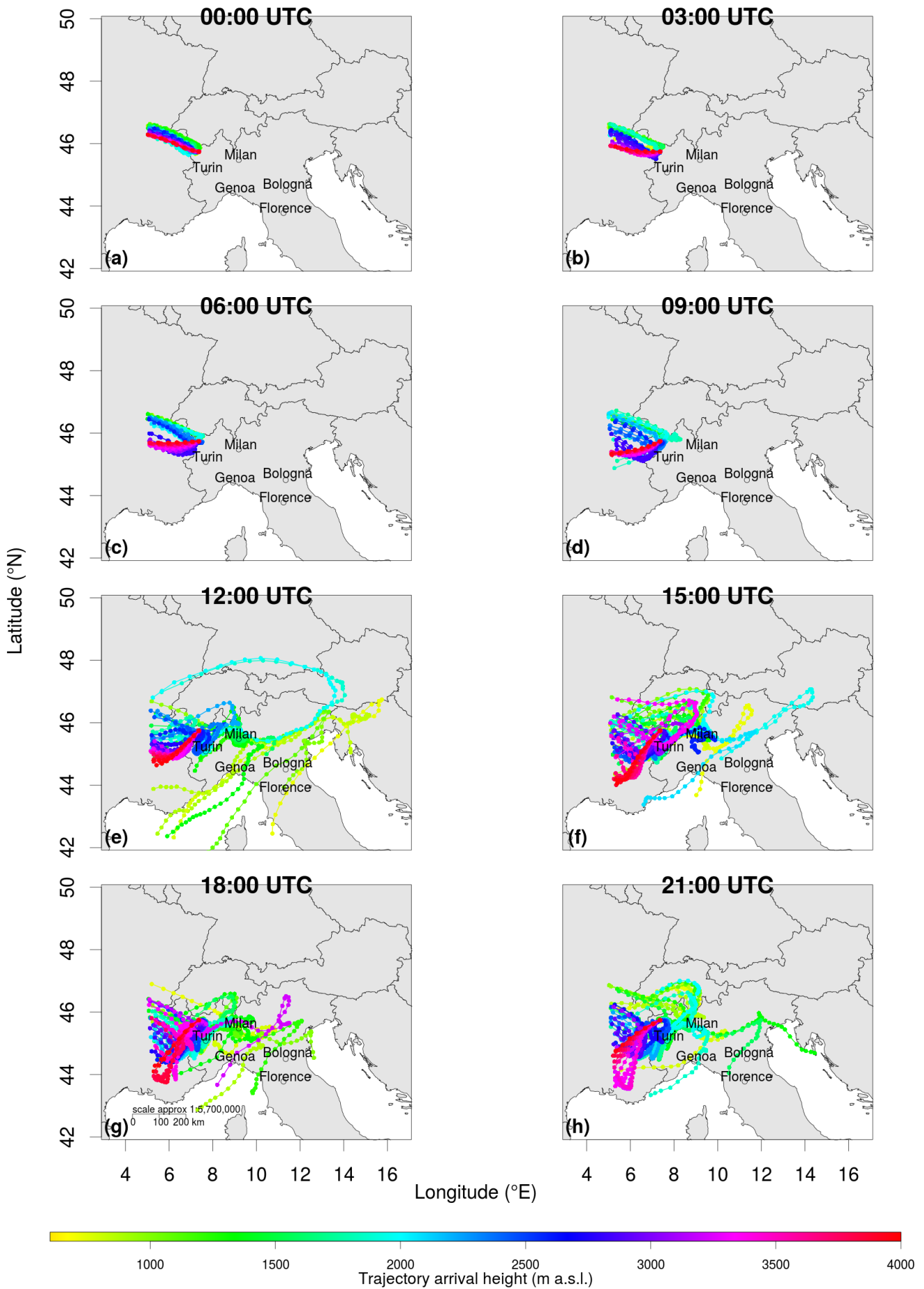
Figure S3: 48-hours back-trajectories ending at Aosta–Saint Christophe on 26 August 2015. The trajectories are cut at the border of the COSMO model. The colour scale represents the arrival height. The dots along each trajectory mark a 1-hour step.

S5 Supporting material to case study 2
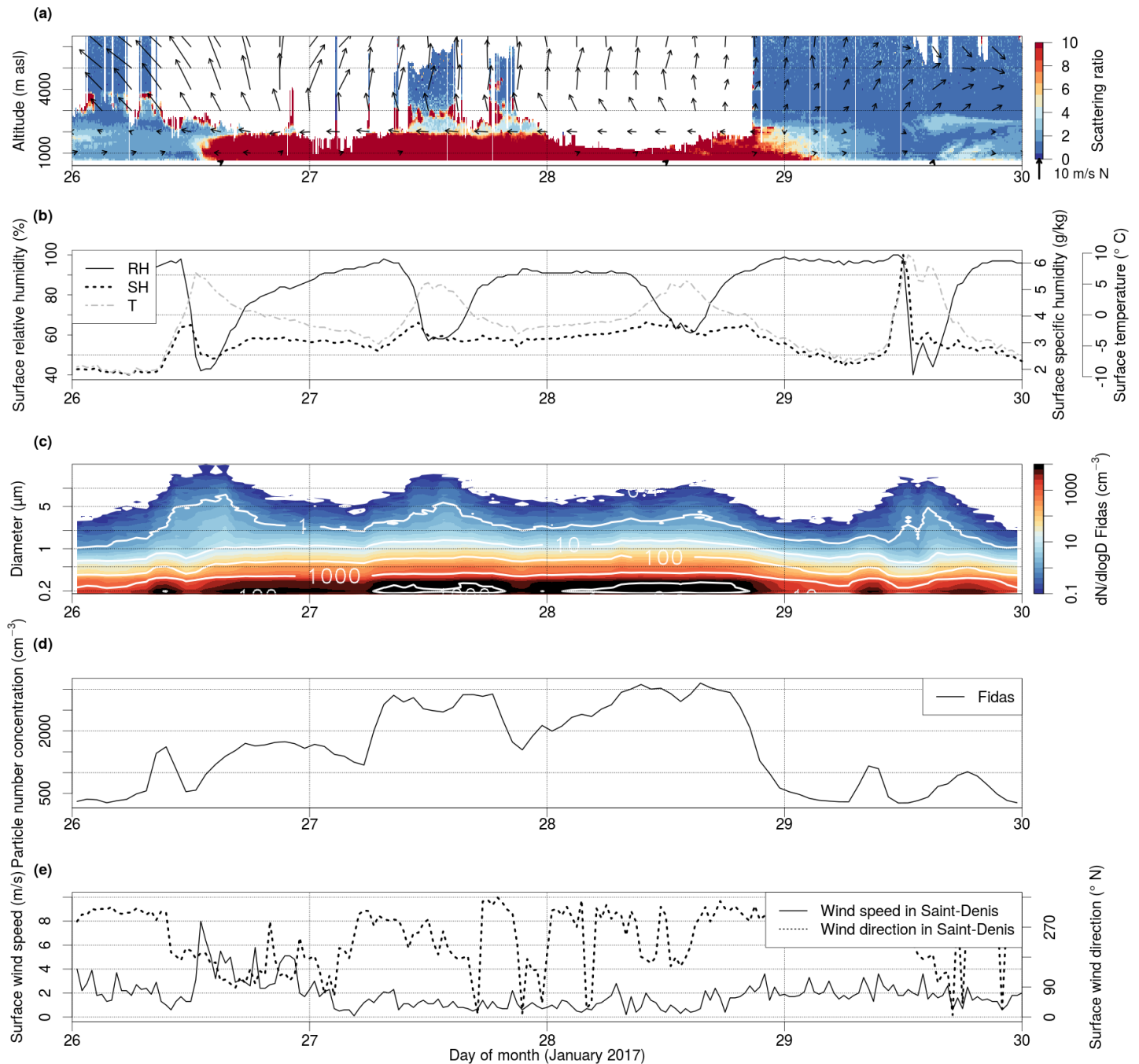
Figure S4: Case study of 26–29 January 2017. (a) Same as in Fig. 10 in the main paper; (b) Surface relative humidity, specific humidity and temperature measured at the Aosta–Saint Christophe weather station; (c) Particle number distribution from the Palas optical counter; (d) Particle number concentration (sum of all channels) from the Palas optical counter; (e) Wind speed and direction at the Saint-Denis station (800 m a.s.l). No data from the photometer are available for the selected period, since the instrument was not operating.
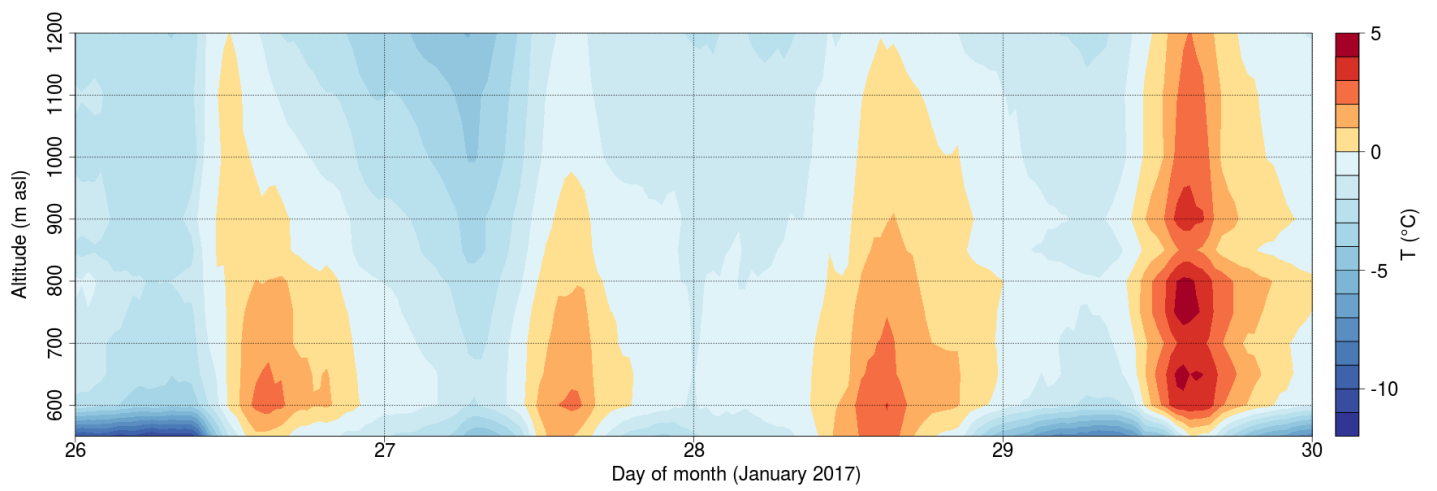
Figure S5: Surface temperature measured along the mountain slope on January 2017.

26 January 2017
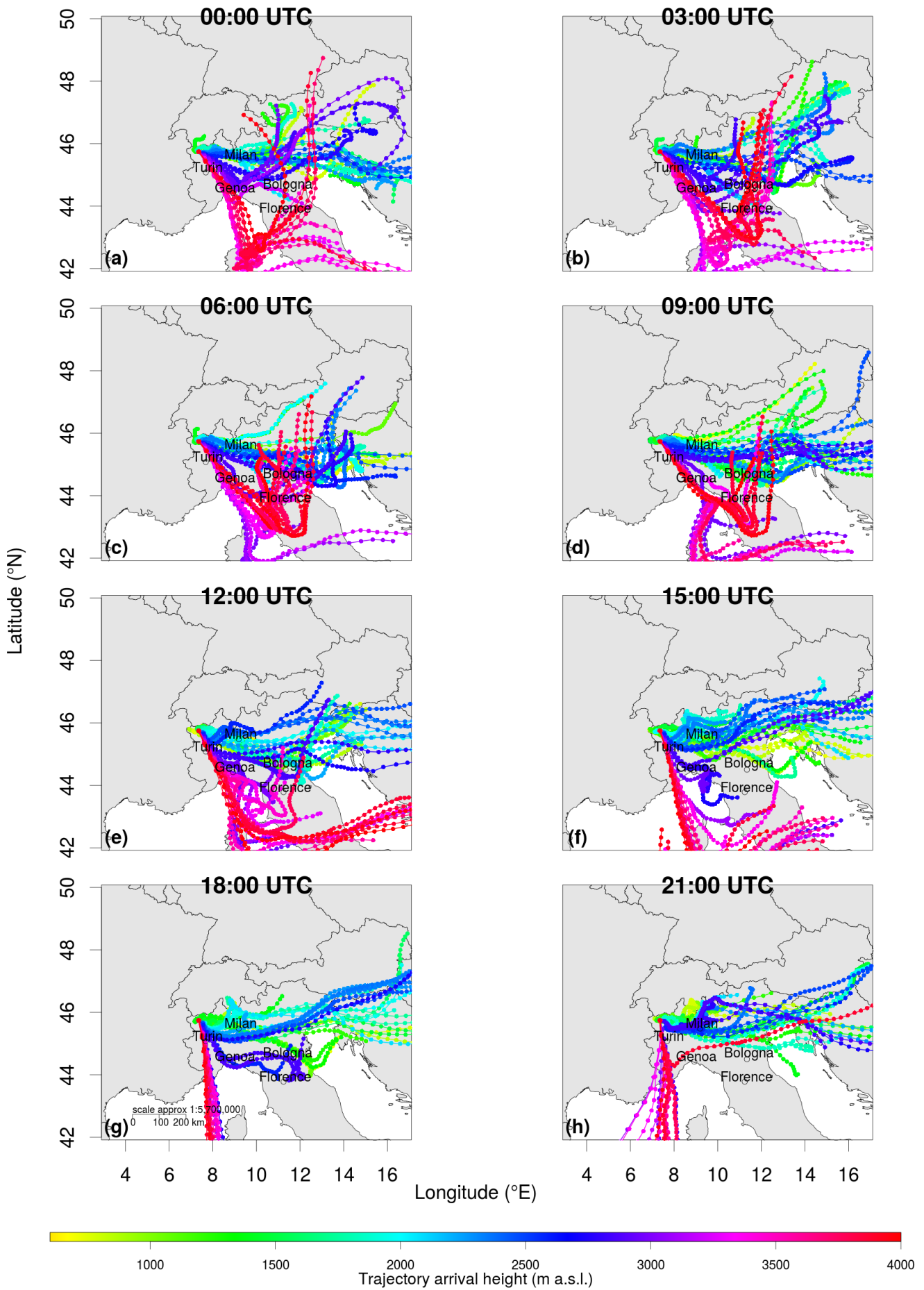
Figure S6: 48-hours back-trajectories ending at Aosta–Saint Christophe on 26 January 2017.
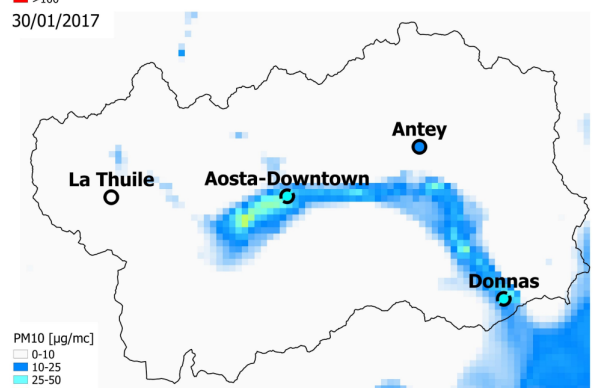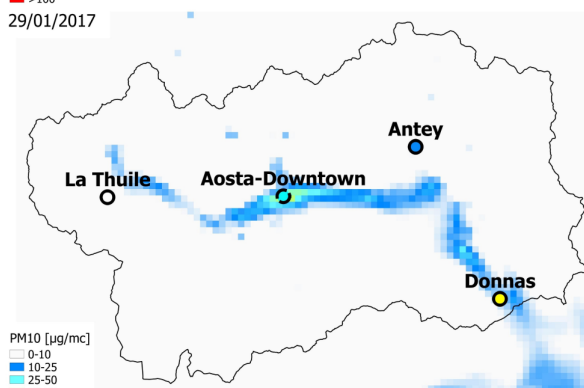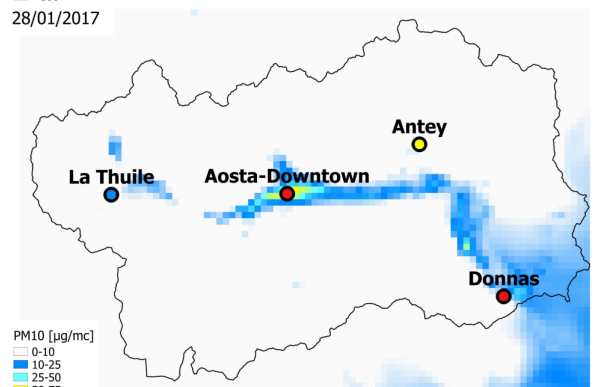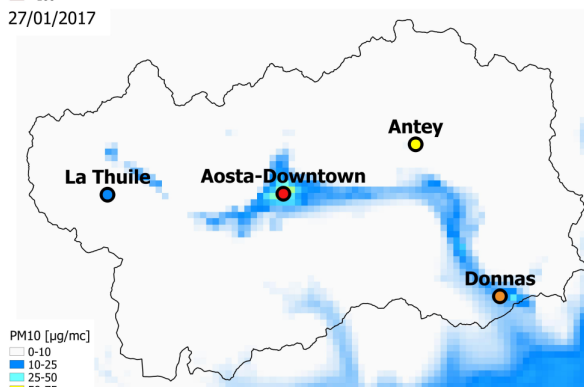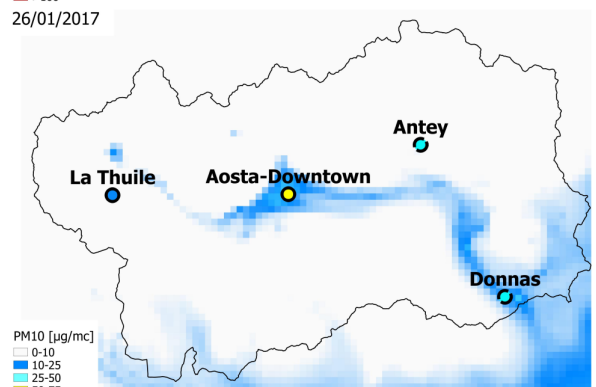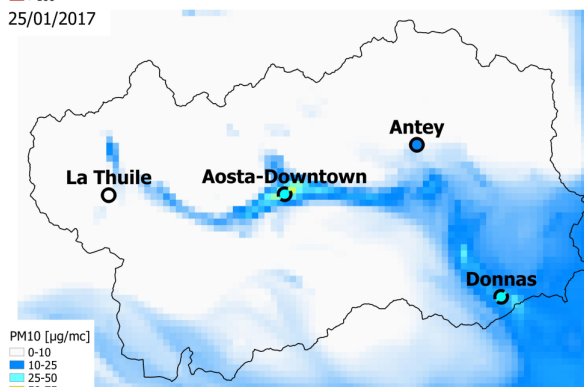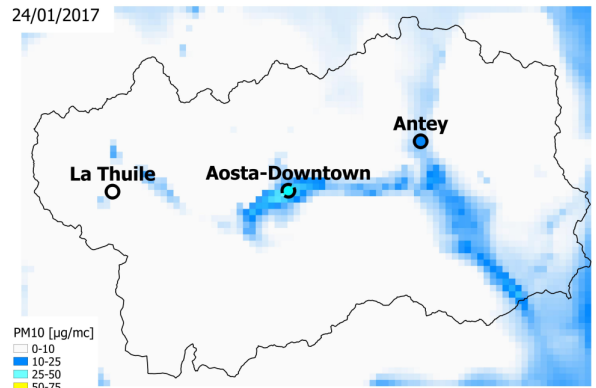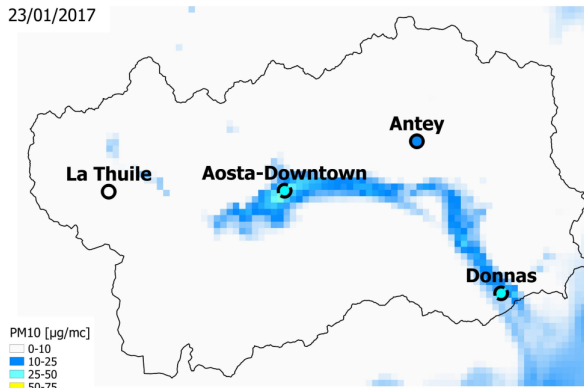
Figure S7: Daily PM$_{10}$ surface (2D) simulations from FARM over the Aosta Valley (background colour) and in-situ measurements (circles) for case sudy 2 (January 2017).

S6 Supporting material to case study 3
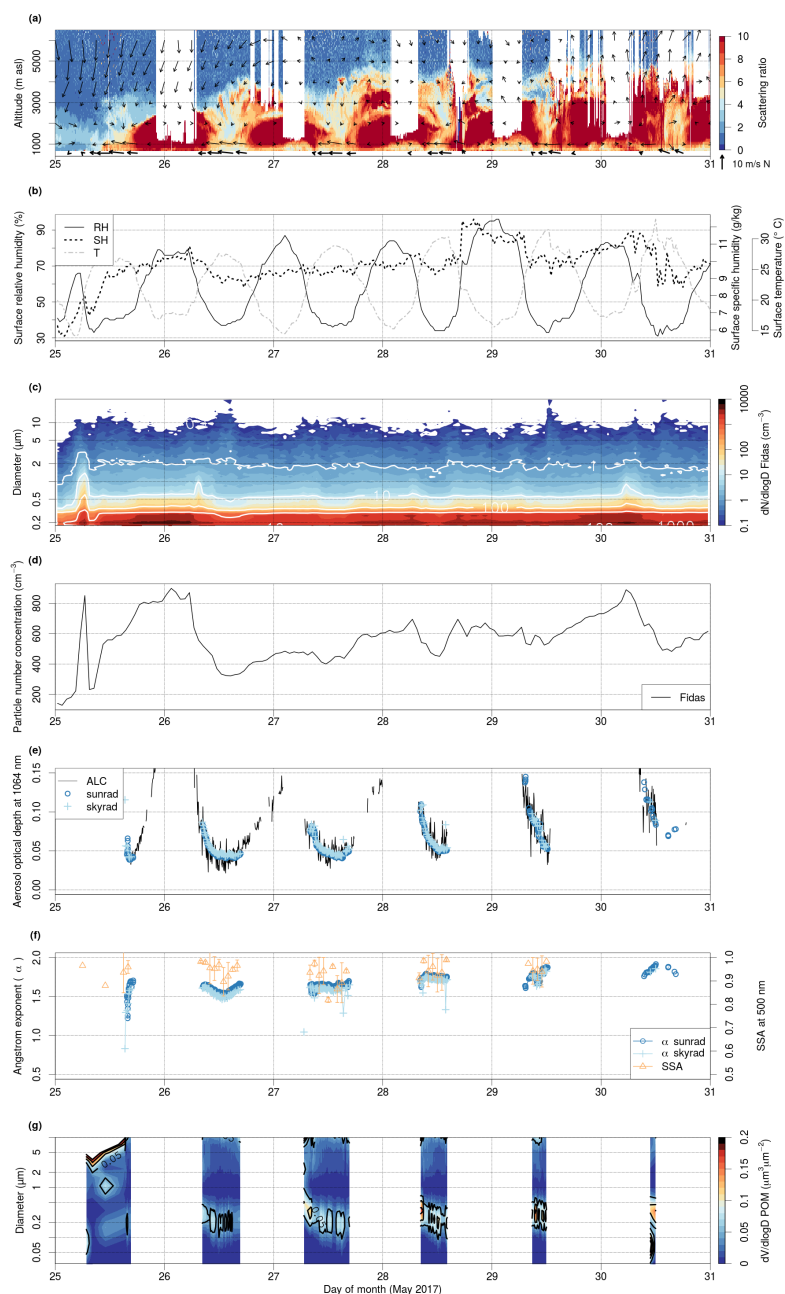
Figure S8: Case study of 25–30 May 2017. (a) Same as in Fig. 13 in the main paper; (b) Surface relative humidity, specific humidity and temperature measured at the Aosta-Saint Christophe weather station; (c) Particle number distribution from the Palas optical counter; (d) Particle number concentration from the Palas optical counter; (e) AOD at 1064 nm from ALC (derived from the functional relationships and filtered for clouds) and photometer (both sunrad and skyrad algorithms); (f) Ångström exponent from both sunrad and skyrad algorithms (left axis), and SSA (right axis) from the photometer; (g) Volume size distribution from the photometer (cut at 10 μm diameter for ease of visualisation of the smallest sizes).

25 May 2017
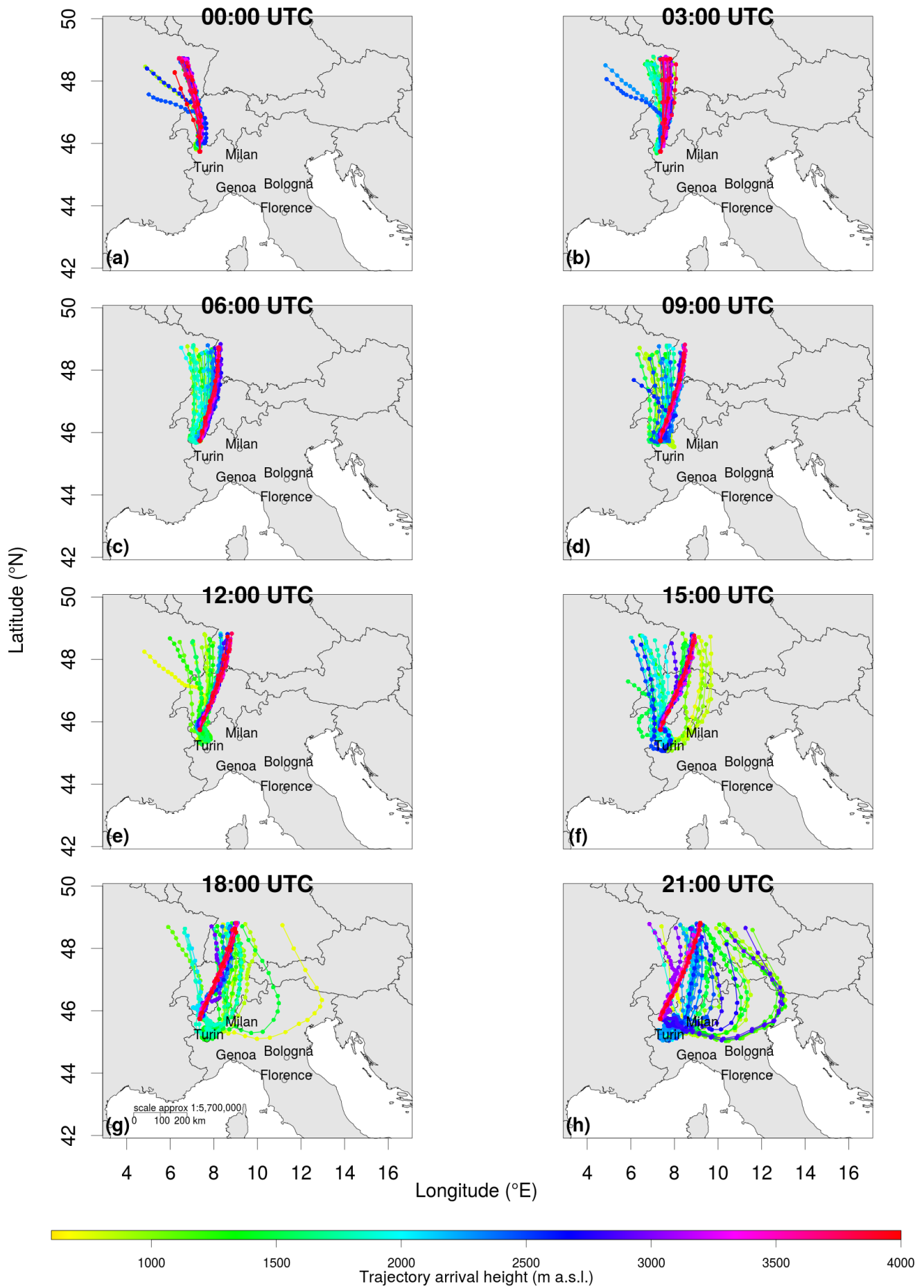
Figure S9: 48-hours back-trajectories ending at Aosta–Saint Christophe on 25 May 2017.

S7 Sensitivity studies on boundary conditions and alternative approach to estimate the hygroscopic effects

This section describes some additional tests that we performed on simulations for case study 1 (August 2015): 1) increase (doubling) of concentrations from the boundary conditions (BC). This large perturbation can be justified by the abrupt change of the national emission inventory grid resolution (12 km) to the local scale (1 km); 2) use of two different schemes, in place of the one employed by FARM, to simulate the aerosol hygroscopic effects. To this purpose, two empirical parametrisations were adopted, since the chemical composition of the elevated aerosol layer is not available experimentally, and might differ from that measured at ground (e.g., Curci et al., 2015), thus thermodynamic equilibrium models (e.g., ISORROPIA) are difficult to employ with the available data.

Figure S10 shows the discrepancy between the concentration profiles retrieved by the ALC (panel a) and the ones initially simulated by FARM (panel b; PM_{10w}, local+remote sources, same as Fig. 13b in the main paper). The results with the modified boundary conditions (test 1) are displayed in Fig. S10c and represent a clear improvement. Notably, transport events at the end of each day are better distinguishable and the concentrations approach to the ones retrieved by the ALC. However, both systematic anticipation of the maximum of each event and absence of the elevated, high-concentration "blobs" visible in the measurements are still noticeable in the panel.

We thus introduced different parametrisations for water uptake by aerosols and applied them to the dry concentrations simulated by FARM with doubled BC. In the first scheme (Fig. S10d), we assumed that the aerosol grow factor (GF), describing the increase of the particle size due to water uptake relative to the dry case, can be approximated by a γ-law function of relative humidity (e.g., Adam et al., 2012),

$$GF = \left(1 - \frac{RH}{100}\right)^{-\gamma} \tag{1}$$

The mass concentration of the moist aerosol (PM_w) can thus be estimated from the dry concentration (PM) as follows:

$$PM_w = PM\left(1 + \frac{\rho_w}{\rho_d}(GF^3 - 1)\right) \tag{2}$$

where ρ_w and ρ_d are pure water and dry aerosol densities, respectively. We assumed a hygroscopic parameter $\gamma = 0.2$, typical of the Po Valley in summer months (Adam et al., 2012), a dry aerosol density $\rho_d = 1.3\ \mathrm{g\,cm^{-3}}$ as already used in our calculations, and we employed the RH profile forecasted by the COSMO model.

In the second scheme (Fig. S10e), we used experimental mass growth obtained in Milan (summer conditions, RH range 30–90%) by D'Angelo et al. (2016). The two experimental branches of the mass growth (for increasing and decreasing RH conditions) were averaged for this test. Additionally, since the simulated RH profiles by COSMO occasionally exceeded 90%, we extrapolated the curve to higher humidities based on a γ-law, fitted to the points with RH$\geq$80% (Fig. S11).

Figures S10d and S10e show the PM_{10w} concentrations obtained with the two methods. As visible from the plots, both the new approaches provide increased PM_{10w} concentration in the elevated layers compared to the FARM output, almost reaching the high values of the measurements. Moreover, the maxima are slightly shifted towards midnight, as desired, since RH maxima are attained later at night than the aerosol advections.

Finally, the results of doubling the concentrations from the boundary conditions during case study 2 (winter case, January 2017) are displayed in Fig. S12.
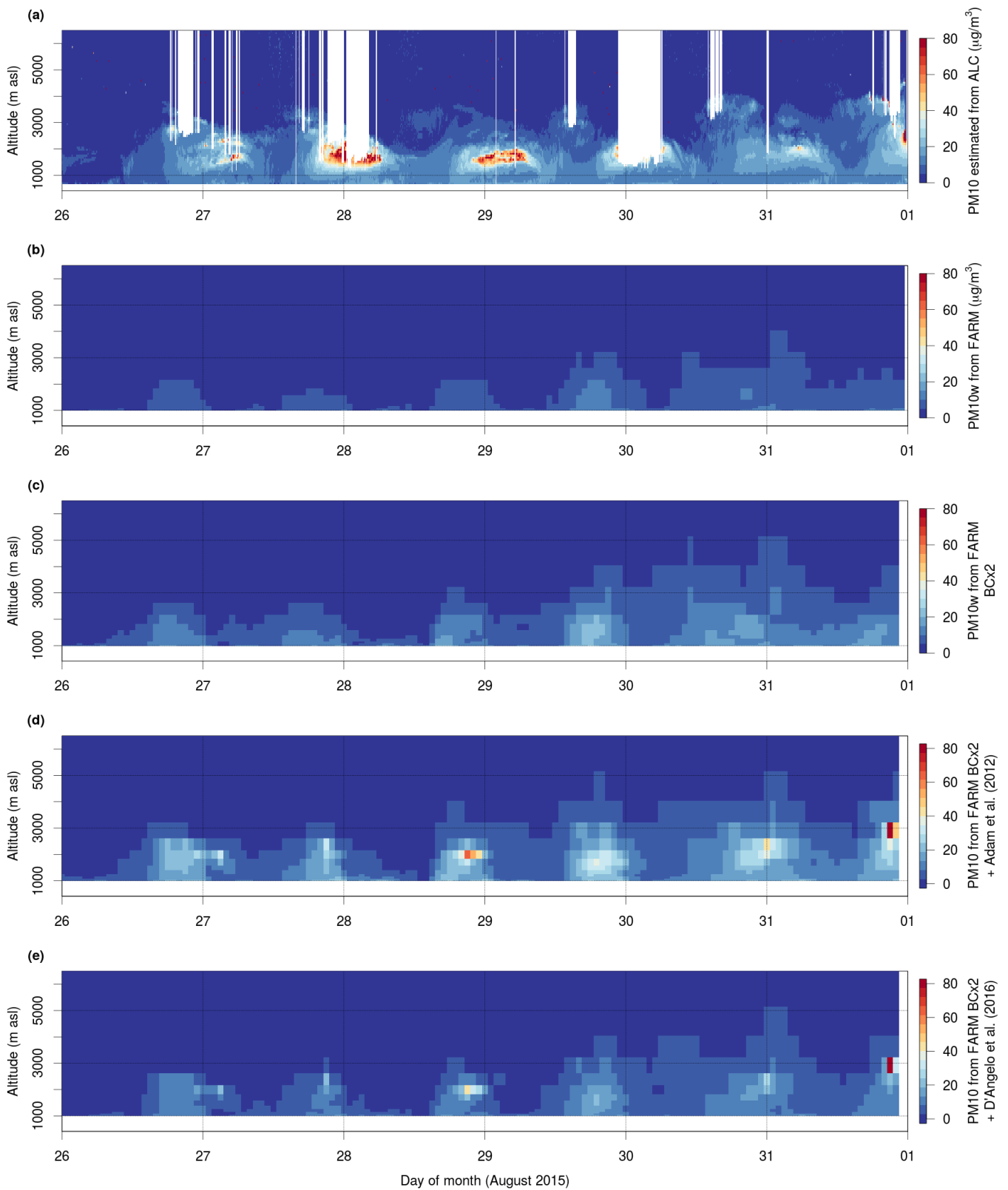
Figure S10: (a) PM_{10} concentration retrieved from ALC measurements; (b) PM_{10w} concentration initially simulated by FARM for the first case study; (c) PM_{10w} concentration simulated by FARM using doubled concentrations from the boundary conditions; (d) hydrated aerosol concentration calculated with the empirical model based on a γ-law (BC still doubled in FARM); (e) hydrated aerosol concentration calculated with the empirical model based on the function represented in Fig. S11 (BC still doubled in FARM).
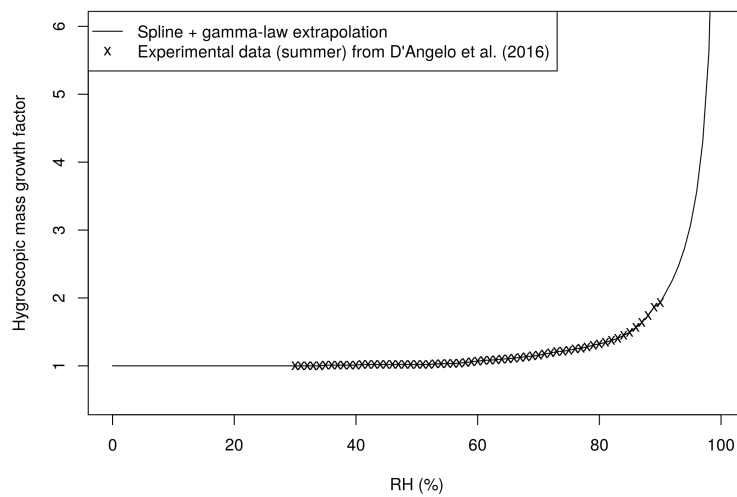
Figure S11: Hygroscopic mass growth factor (crosses) from measurements by D'Angelo et al. (2016). The continuous line represent an interpolation within the range of observations (30–90%) and an extrapolation using a γ-law to higher values of RH.
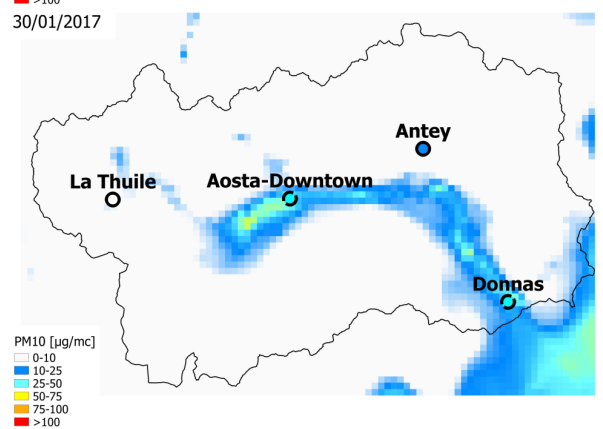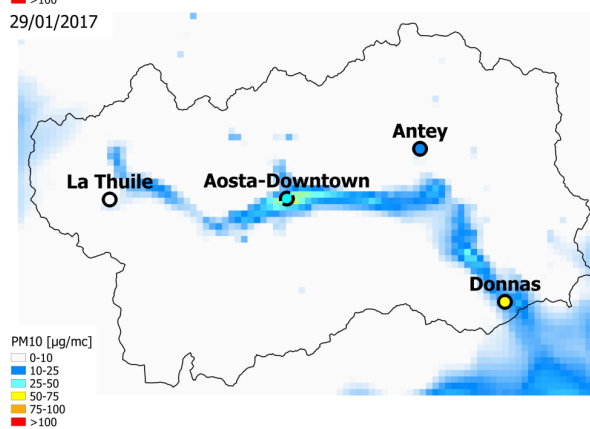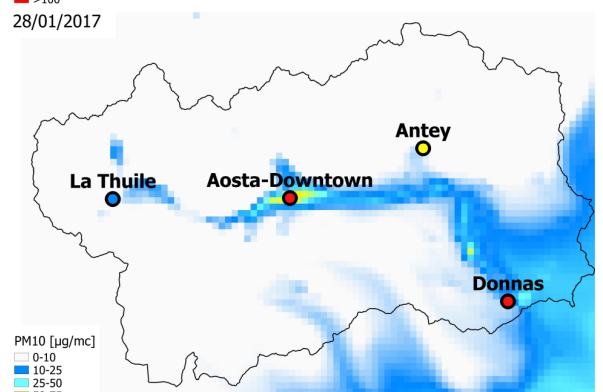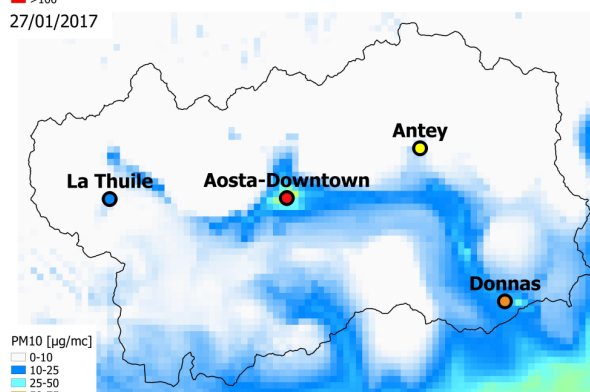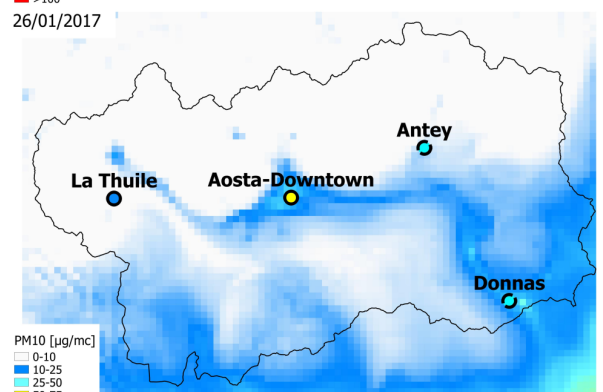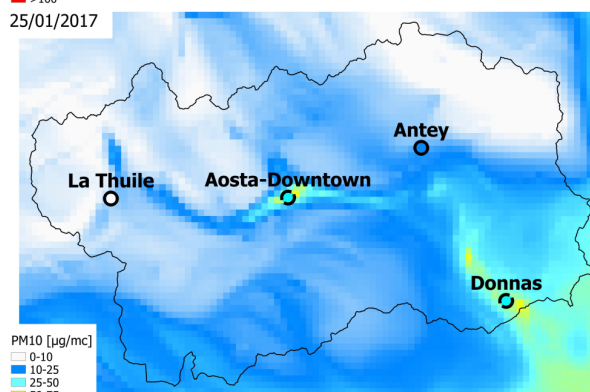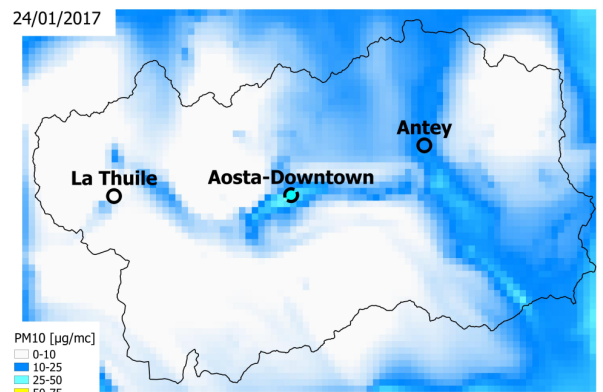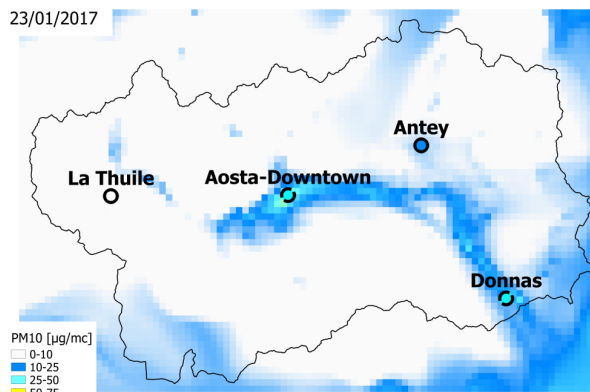
Figure S12: Same as Fig. S7, with doubled concentrations from outside the regional boundaries of the Aosta Valley.

References

Adam, M., Putaud, J. P., Martins dos Santos, S., Dell'Acqua, A., and Gruening, C.: Aerosol hygroscopicity at a regional background site (Ispra) in Northern Italy, Atmos. Chem. Phys., 12, 5703–5717, doi:10.5194/acp-12-5703-2012, 2012.

Baklanov, A., Lawrence, M., Pandis, S., Mahura, A., Finardi, S., Moussiopoulos, N., Beekmann, M., Laj, P., Gomes, L., Jaffrezo, J.-L., Borbon, A., Coll, I., Gros, V., Sciare, J., Kukkonen, J., Galmarini, S., Giorgi, F., Grimmond, S., Esau, I., Stohl, A., Denby, B., Wagner, T., Butler, T., Baltensperger, U., Builtjes, P., van den Hout, D., van der Gon, H. D., Collins, B., Schluenzen, H., Kulmala, M., Zilitinkevich, S., Sokhi, R., Friedrich, R., Theloke, J., Kummer, U., Jalkinen, L., Halenka, T., Wiedensholer, A., Pyle, J., and Rossow, W. B.: MEGAPOLI: concept of multi-scale modelling of megacity impact on air quality and climate, Adv. Sci. Res., 4, 115–120, doi:10.5194/asr-4-115-2010, 2010.

Curci, G., Ferrero, L., Tuccella, P., Barnaba, F., Angelini, F., Bolzacchini, E., Carbone, C., Denier van der Gon, H. A. C., Facchini, M. C., Gobbi, G. P., Kuenen, J. P. P., Landi, T. C., Perrino, C., Perrone, M. G., Sangiorgi, G., and Stocchi, P.: How much is particulate matter near the ground influenced by upper-level processes within and above the PBL? A summertime case study in Milan (Italy) evidences the distinctive role of nitrate, Atmos. Chem. Phys., 15, 2629–2649, doi:10.5194/acp-15-2629-2015, 2015.

D'Angelo, L., Rovelli, G., Casati, M., Sangiorgi, G., Perrone, M. G., Bolzacchini, E., and Ferrero, L.: Seasonal behavior of PM2.5 deliquescence, crystallization, and hygroscopic growth in the Po Valley (Milan): Implications for remote sensing applications, Atmos. Res., 176-177, 87 – 95, doi:10.1016/j.atmosres.2016.02.011, URL http://www.sciencedirect.com/science/article/pii/S016980951630028X, 2016.

EEA: EMEP/EEA air pollutant emission inventory guidebook 2016 – Technical guidance to prepare national emission inventories, Tech. rep., European Environment Agency, doi:10.2800/247535, 2016.

Kukkonen, J., Olsson, T., Schultz, D. M., Baklanov, A., Klein, T., Miranda, A. I., Monteiro, A., Hirtl, M., Tarvainen, V., Boy, M., Peuch, V.-H., Poupkou, A., Kioutsioukis, I., Finardi, S., Sofiev, M., Sokhi, R., Lehtinen, K. E. J., Karatzas, K., San José, R., Astitha, M., Kallos, G., Schaap, M., Reimer, E., Jakobs, H., and Eben, K.: A review of operational, regional-scale, chemical weather forecasting models in Europe, Atmos. Chem. Phys., 12, 1–87, doi:10.5194/acp-12-1-2012, 2012.

Menut, L. and Bessagnet, B.: Atmospheric composition forecasting in Europe, Ann. Geophys., 28, 61–74, doi:10.5194/angeo-28-61-2010, 2010.

Pession, G., Magri, T., Zublena, M., Agnesod, G., Genon, G., Blanc, L., Silibello, C., Finardi, S., Calori, G., and Nanni, A.: Dust generation and dispersion (PM10 and PM2. 5) in the Aosta Valley: analysis with the FARM model, Hrvatski meteorološki časopis, 43, 603–607, URL http://hrcak.srce.hr/file/96455, 2008.

Pession, G., Magri, T., Calori, G., Costa, M., Bande, S., Bissardella, S., and Clemente, M.: Integrated source apportionment in support of Aosta valley and Piemonte air quality plans, in: Proceedings of Abstracts 10th International Conference on Air Quality Science and Application, Milano, University of Hertfordshire College Lane, 2016.

Pignatelli, T., De Lauretis, R., Contaldi, M., D'Elia, I., Romano, D., and Vialetto, G.: Harmonization of National inventory and projections of multi-pollutant emission scenarios. The Italian experience within the European context and the UN-ECE Convention on Long Range Transboundary Air Pollution, in: Proc. of 16th Annual Int. Emissions Inventory Conference, Raleigh (North Carolina), URL https://www3.epa.gov/ttnchie1/conference/ei16/session8/pignatelli.pdf, 2007.

Silibello, C., Finardi, S., Pittini, T., Pession, G., and Magri, T.: Model based yearly air quality evaluation on a very complex terrain alpine region (Valle d'Aosta), in: Proc. of the 11th Int. Conf. on Harmonization, Cambridge, UK, pp. 2–5, URL http://www.harmo.org/conferences/proceedings/_Cambridge/publishedSections/Pp281-285.pdf, 2007.

Taurino, E., Bernetti, A., De Lauretis, R., D'Elia, I., Di Cristofaro, E., Lena, F., Gagna, A., Gonella, B., Pantaleoni, M., Peschi, E., Romano, D., and Vitullo, M.: Italian emission inventory 1990-2014 – Informative inventory report 2016, 2016.